Applied Catalysis B: Environmental 156–157 (2014) 341–349

Contents lists available at ScienceDirect

Applied Catalysis B: Environmental

journal homepage: www.elsevier.com/locate/apcatb

Highly efficient cathode catalyst layer based on nitrogen-doped carbon nanotubes for the alkaline direct methanol fuel cell

Petri Kanninen[a], Maryam Borghei[b], Olli Sorsa[a], Elina Pohjalainen[a], Esko I. Kauppinen[b], Virginia Ruiz[b,c], Tanja Kallio[a,*]

[a] Department of Chemistry, Aalto University, P.O. Box 16100, 00076 Aalto, Finland
[b] Department of Applied Physics, Aalto University, P.O. Box 15100, 00076 Aalto, Finland
[c] IK4-CIDETEC – Centre for Electrochemical Technologies, Paseo Miramón 196, E-20009 Donostia-San Sebastián, Spain

ARTICLE INFO

Article history:
Received 29 November 2013
Received in revised form 14 March 2014
Accepted 22 March 2014
Available online 31 March 2014

Keywords:
Oxygen reduction
Direct methanol fuel cell (DMFC)
Alkaline membrane electrolyte
Nitrogen-doping
Carbon nanotube

ABSTRACT

The performance of a direct methanol alkaline anion-exchange membrane (Fumatech FAA3) fuel cell with Pt-free nitrogen-doped few-walled carbon nanotubes (N-FWCNT) as the cathode catalyst is compared with a commercial supported Pt catalyst. The ionomer content of the N-FWCNT cathode catalyst layer is therefore optimized and it is shown to be 40 wt% of FAA3. Scanning electron microscopy images of the catalyst layer show that the ionomer forms aggregates with N-FWCNTs probably due to their charged nature and that the catalyst layer structure is remarkably open even with high ionomer contents facilitating the mass transfer of reactants and products to the active sites. With oxygen as the oxidant, the maximum power density obtained with our Pt-free N-FWCNTs (0.78 mW cm^{-2}) is slightly higher than with the Pt catalyst (0.72 mW cm^{-2}). However, when more practical air is used as the oxidant, the N-FWCNTs (0.73 mW cm^{-2}) show clearly superior performance compared to the Pt catalyst (0.18 mW cm^{-2}). The lower performance with the Pt catalyst is attributed to the denser electrode layer structure resulting in higher mass transport resistance and to the presence of methanol in the cathode, which poisons the Pt but not the N-FWCNTs.

1. Introduction

Liquid-fed fuel cells, like the direct methanol fuel cell (DMFC), are very promising candidates for power sources of low-power electronic devices. However, large-scale commercialization requires improvements in the performance, durability and cost of the catalysts [1] and membranes [2]. Many activities are concentrated on the anode where complex and relatively slow methanol oxidation occurs, but the oxygen reduction reaction (ORR) taking place at the cathode is also under active research, especially since all typical fuel cells employ an oxygen reducing cathode. Although ORR is catalyzed relatively well by platinum, large loadings are required (0.4 mg cm^{-2}) due to the complexity of the reaction compared with for example hydrogen oxidation (0.05 mg cm^{-2}) [3]. This contributes greatly to the total cost of the whole system. Platinum nanoparticles used as catalysts also agglomerate during fuel cell use further reducing their activity [4]. In addition with DMFCs, methanol crossover from the anode to the cathode due to unideal membrane materials causes a mixed potential and poisons the catalyst in the cathode with the intermediate product CO [5].

To solve these problems, alternative catalyst materials for ORR have been researched [6–9]. Recently, nitrogen-modified carbon materials have been shown to have inherent oxygen reduction activity that can reach or even exceed the activity of Pt-catalysts, while being immune to CO and methanol poisoning, and catalyst nanoparticle agglomeration [10–12]. These catalysts show moderate activity toward oxygen reaction in acidic and neutral conditions, and excellent activity in alkaline conditions [13–17]. Generally, they have been synthesized with the help of metal catalysts (e.g. Co or Fe), which had raised the concern that the ORR activity was attributable to the metal-nitrogen complexes as in the well-known case of metal-porphyrins [9]. However, synthesis methods that do not use any metal precursors or catalysts have been recently developed and ORR activity of the catalyst has been preserved [15,18–22].

The exact mechanism of the ORR on nitrogen-modified carbon is not entirely clear at the moment, but the active sites are generally thought to be quaternary nitrogen atoms bonded to three carbons and pyridinic ones bonded to two carbons, or the highly active defect and edge sites present near the nitrogens functionalities [6].

* Corresponding author. Tel.: +358 50 5637567; fax: +358 9 47022580.
E-mail address: tanja.kallio@aalto.fi (T. Kallio).

http://dx.doi.org/10.1016/j.apcatb.2014.03.041
0926-3373/

Also, the more electronegative nature of nitrogen compared to carbon causes a negative charge on the nitrogen atom and positive charges on the surrounding carbon atoms, which should facilitate the adsorption of O_2 on the catalyst surface [11].

Although a large number of metal-free N-modified materials have been synthesized and studied for ORR (e.g. graphene [10,23–33], carbon nanotubes [11,20,21,34–43], carbon nanofibers [12,44–47], mesoporous carbon [15,22], graphitic carbon [48,49], carbon spheres [19,50–53], carbon nanocages [54], flower-like carbon [55], carbon aerogel [56,57], vesicular carbon [58], nanodiamonds [59]) relatively few have been tested in actual fuel cell conditions [58,60–69].

The most popular application target is the acidic polymer electrolyte membrane fuel cell (PEMFC) using hydrogen fuel. Nallathambi et al. [60] showed that metal-free synthesis of N-functional groups containing carbon black improved its ORR activity compared to as-received carbon material. Pyrolysis of the catalyst with a Co–Fe(1:1) chelate complex followed by acid-leaching to remove the metals further improved its performance, while the voltage loss for the catalyst over a 480 h test was 80 $\mu V\,h^{-1}$. Wu et al. [61] found similar results with N-doped graphene nanoplatelets, which contained very little Fe (0.6 at%) and no Co residues on the surface of the catalyst. The catalyst showed somewhat poorer performance than a Pt catalyst (80 mV lower potential at 0.1 A cm^{-2}) and good stability over 400 h (voltage loss of 100 $\mu V\,h^{-1}$). Mo et al. [58] synthesized N-doped metal-free vesicular carbon with a Fe catalyst and showed maximum power density of 200 mW cm^{-2}, while commercial Pt-catalyst produced 550 mW cm^{-2} in the same conditions. Onodera et al. [62] synthesized N-doped carbon on KetjenBlack support, which showed moderate performance in a PEMFC. Oh et al. [63] modified carbon black, carbon nanotubes and carbon nanofibers with nitrogen and showed that the nanofibers performed best in a H_2/O_2 fuel cell due to their high nitrogen content and edge plane exposure. The performance decrease of the fuel cell was 215 $\mu A\,cm^{-2}\,h^{-1}$ over a 120 h test at 0.4 V. Liu et al. [64] studied the nitrogen structure of a N-modified carbon before and after a H_2/O_2 fuel cell test of 100 h and they linked the stability of the catalyst to the quarternary nitrogens, while pyridinic nitrogens protonate under the acidic conditions and become inactive. Similar conclusion about durability was made by Dorjgotov et al. [65] and they also showed performance equivalent of Pt catalyst in H_2/O_2 fuel cell (0.52 A cm^{-2} at 0.6 V).

Recently, alkaline anion-exchange membrane fuel cells (AAMFC) have been studied to replace the expensive Nafion membrane, reduce the corrosion in the fuel cell system and facilitate the catalysis of the electrode reactions [70,71]. Because of the higher ORR activity and stability of the N-modified carbon materials in alkaline conditions [13–17], they have recently been investigated as AAMFC cathodes.

Rao and Ishikawa [66] fabricated N-doped carbon nanotubes with an aluminum template and studied them in an H_2/O_2 AAMFC. The performance of their catalyst was approximately 60% of a Pt catalyst in terms of maximum power density and it was stable for a 30-h test at a constant current. Higgings and Chen [67] synthesized self-standing, acid-washed N-doped carbon nanotube thin films with an Fe catalyst. The catalyst was tested in a H_2/O_2 AAMFC and showed 34% higher maximum power density than carbon supported Pt catalyst.

Although N-modified carbon materials could be highly beneficial for the DMFC due to their tolerance to methanol and CO poisoning [72], there have been only two tests in an actual DMFC. Kim et al. [68] studied nitrogen-doped carbon nanofibers in an acidic DMFC cathode and could generate moderate electrical current. Sun et al. [69] co-doped cheap carbon black materials with nitrogen and fluorine and used them as ORR catalysts in a direct methanol AAMFC. They demonstrated better performance than commercially Pt/C at same catalyst loading (15 vs 13 mW cm^{-2}) and stable performance for 24 h. In another similar study, Mazin et al. [73] used Co and Fe supported on nitrogen-modified carbons in a direct ethanol AAMFCs. They did not report on the performance of the catalyst after acid-leaching to remove the Co and Fe particles.

Other type of fuel cells where metal-free N-modified catalysts have been used as cathodes are microbial fuel cells in neutral conditions resulting in better performance than with Pt [74,75] and intermediate temperature (75–250 °C) fuel cells based on metal oxide electrolytes in both acid and alkaline mode [76].

In this study, we have fabricated MEAs for a direct methanol AAMFC with Pt-free, nitrogen-doped few-walled carbon nanotubes (N-FWCNTs) that have been proven to be very active for ORR in rotating disk electrode measurements [77] as the cathode catalyst and have optimized the ionomer content of the cathode electrode layer. After optimization, we demonstrate that our AAMFC with the N-FWCNT cathode catalyst shows superior performance compared to a commercial carbon supported Pt, both with oxygen and air as the oxidant.

2. Experimental

2.1. Catalyst preparation

A detailed description of the synthesis is given in [77]. Briefly, few-walled carbon nanotubes (FWCNT) were synthesized via decomposition of CH_4 diluted with H_2 at 950 °C on CoMo–MgO catalyst [78]. The FWCNTs were purified by washing in HCl followed by rinsing with deionized water. Nitrogen doping of the FWCNTs was accomplished by first coating them with a layer of polyaniline (PANI) deposited by in situ chemical polymerization of aniline in acidic media and subsequent carbonization of the PANI-coated FWCNTs at 900 °C for 1 h in Ar gas flow, according to a method previously reported for carbon black [79], producing the nitrogen-doped FWCNTs (N-FWCNTs).

High-resolution transmission electron microscopy (HRTEM) was performed on the N-FWCNTs using a double-aberration corrected JEOL-2200FS microscope equipped with a field emission gun operated at 200 kV.

2.2. MEA preparation

FAA3 membrane (Fumatech) was ion-exchanged in 0.5 M NaOH with stirring for 1 h and washed in deionized water. Before assembling the fuel cell, the membrane was soaked in 1 M methanol. The cathode catalyst inks were prepared by mixing the synthesized N-FWCNTs with isopropanol and 12 wt% solution of FAA3 ionomer in N-methyl-2-pyrrolidone (NMP). The amount of FAA3 was varied so that its weight percentage of the total cathode mass (ionomer + N-FWCNT) was 21.7, 30.6, 42.0, 51.1 and 60.5 wt% in each case. The MEAs fabricated from the above inks were labeled as MEA20, MEA30, MEA40, MEA50 and MEA60, respectively. The components were first mixed by a magnetic stirrer for 45 min, then subjected to 10 min of sonication and finally mixed by a magnetic stirrer overnight. Isopropanol (400–600 μl) was added to the ink during mixing until the viscosity of the ink was suitable for air brush painting: the more FAA3 solution in the ink, the less isopropanol was needed for good viscosity. The resulting slurry was painted on a pre-weighted gas diffusion layer (GDL) with a microporous layer (FuelCellEtc GDL-CT) by an air brush and dried in a vacuum oven at 40 °C for 1 h. The GDL was then weighed to determine the weight of the dry catalyst layer. The N-FWCNT loadings of the cathodes were 2.2 ± 0.3 mg cm^{-2}. The same procedure was used to fabricate a reference MEA with Pt supported on a high surface area carbon (Alfa Aesar, 60 wt% Pt). The FAA3 content in this case was 30 wt%

according to the optimized value reported by Carmo et al. [80] and the Pt loading was 0.5 mg cm^{-2}.

The anode electrodes for the MEAs were fabricated from PtRu supported on high surface area carbon (Alfa Aesar, 40 wt% Pt, 20 wt% Ru) with similar method as the cathodes. The FAA3 ionomer content in this case was 30 wt% [80] and the PtRu loading was 3.0 ± 0.2 mg cm^{-2}. A higher PtRu loading and lower N-FWCNT loading was used to ensure that the catalytic activity of the fuel cell would be limited by the cathode only. The MEAs were not hot-pressed due to the sensitivity of the FAA3 membrane to pressure and temperature [80].

2.3. Fuel cell measurements

The fuel cell was assembled with a FAA3 membrane, painted electrodes and Teflon® gaskets. The cell was then clamped together with eight screws and tightened to a torque of 5 Nm. The active area of the fuel cell was 5.29 cm^2. Cell voltage and current were controlled by a Metrohm Autolab PGSTAT20 potentiostat with a BSTR10A booster. Prior to the measurement, the cell was first allowed to activate overnight at 50 °C, with a 0.2 ml min^{-1} flow of 1 M methanol solution in deionized water at the anode and 100 ml min^{-1} flow dry O_2 (5.0, Aga) at the cathode, while constant current of 0.5 mA cm^{-2} was applied.

The next day, the flow rates of methanol and O_2 were increased to 2.0 ml min^{-2} and 200 ml min^{-2}, respectively. Once the open circuit voltage (OCV) stabilized, polarization curves were measured with a voltage sweep from the OCV to 0.05 V at a rate of 2 mV s^{-1}. Then synthetic air (80% N_2, 20% O_2) was changed to the cathode, the cell was let to stabilize for 30 min and a new set of polarization curves were recorded.

Next, impedance measurements were performed. The methanol solution at the anode was replaced with humidified H_2 (5.0, Aga) to minimize the anode overpotential and O_2 humidified at 50 °C was fed to the cathode. The impedance spectrum of the whole cell was then measured at OCV from 100 kHz to 10 mHz using a 0.25 mA sinusoidal signal. Polarization curves were also measured with H_2 fuel with O_2 and synthetic air at the cathode.

Finally, a chronoamperometric measurement for 6 h was made. Methanol solution was fed to the anode at 0.4 ml min^{-1} and oxygen to the cathode at 100 ml min^{-1} for 1 h. One polarization curve was measured to ensure that all the H_2 at the anode was oxidized and then a constant voltage measurement at 0.2 V was started.

After the fuel cell was dismantled, two samples for scanning electron microscopy (SEM) were cut from the cathode catalyst layer: one from the center of the MEA and one close to the edge of the MEA. A JEOL JSM-7500FA field emission scanning electron microscope was used for the measurements.

3. Results and discussion

3.1. N-FWCNT properties

Morphology of the N-FWCNTs was analyzed by HR-TEM (Fig. 1). The pristine samples (Fig. 1a) consist of 2–5 walls up to 6 nm diameter and about 1 μm length attached together in bundles and the morphology of N-FWCNTs does not differ significantly from that of the undoped ones. The nitrogen content determined by X-ray photoelectron spectroscopy (XPS) was found to be relatively low, 0.56 at%, which implies that doping has not considerably altered the bulk properties of the pristine material. A full characterization of N-FWCNTs can be found in our paper [77]. After the fuel cell testing, no significant differences in the N-FWCNT structure can be seen in the TEM images (Fig. 1b). Small clusters of amorphous material are attached to the N-FWCNTs, which is most likely the FAA3 ionomer that was not separated from the nanotubes during the sample preparation.

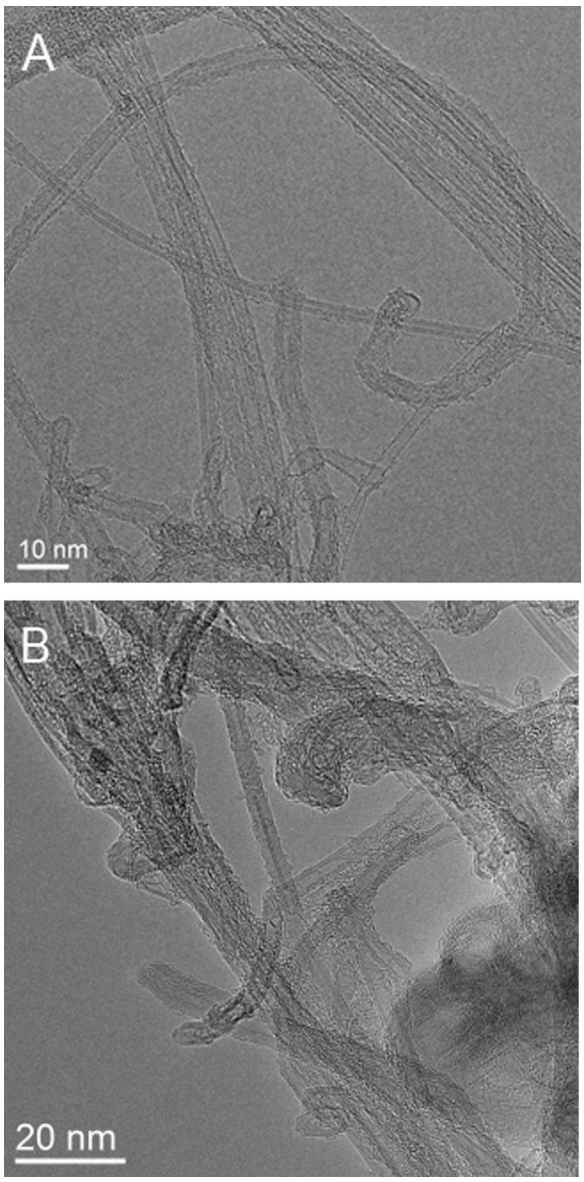

Fig. 1. TEM images of the (A) pristine and (B) used N-FWCNTs.

3.2. Cathode catalyst layer optimization

The optimum cathode catalyst layer structure was studied by fabricating MEAs with different FAA3 contents and measuring their performance in an alkaline anion-exchange membrane fuel cell using methanol as the fuel and oxygen and synthetic air as the oxidant. Previous studies have shown that catalysts supported by high aspect ratio carbon materials require high amounts of ionomer in the catalyst layer (>50 wt%) for optimal performance [81–83] and that for a H_2-fueled, FAA3-based fuel cell with a commercial carbon-supported catalyst the optimum ionomer content is around 25 wt% [80]. Thus, it was decided to study the performance of the DMFC in a wide ionomer content range from 20 wt% to 60 wt% of the cathode catalyst layer. Polarization curves and power density curves of the MEAs with oxygen at the cathode are presented in Fig. 2 and Table 1. It can be seen that 40 wt% of FAA3 in the cathode catalyst layer (MEA40) resulted in the best performance: both the current density at 0.05 V (9.1 mA cm^{-2}) and maximum power

Table 1
The properties and performances of the investigated MEAs.

MEA	P_{max} (O_2)[a] (mW cm^{-2})	$I_{0.05\,V}$ (O_2)[b] (mA cm^{-2})	P_{max} (air)[a] (mW cm^{-2})	$I_{0.05\,V}$ (air)[b] (mA cm^{-2})	Stability[c] (μA cm^{-2} h^{-1})	Resistance[d] (Ω cm^2)	Thickness[e] (μm)
MEA20	0.55	6.3	0.53	5.5	49	1.309	N/A
MEA30	0.68	8.0	0.64	6.8	42	0.612	80 ± 17
MEA40	0.78	9.1	0.73	7.8	45	0.671	116 ± 17
MEA50	0.70	7.9	0.65	6.7	41	0.753	97 ± 11
MEA60	0.60	6.8	0.56	5.8	43	0.773	127 ± 14
MEA-Pt	0.72	8.9	0.18	2.7	N/A	0.830	19 ± 4

[a] DMFC maximum power density.
[b] DMFC current density at cell voltage of 0.05 V.
[c] DMFC current decrease over 6 h at cell voltage 0.2 V.
[d] Total cell resistance determined from high frequency impedance at 9.5 mA cm^{-2}.
[e] Average cathode catalyst layer thickness and standard deviation determined from the SEM images (6 measurement points per MEA).

density (0.78 mW cm^{-2}) are higher than with the other MEAs. The trend of the maximum power density against the FAA3 content exhibits a clear maximum at 40 wt% (Fig. 3).

When the oxidant is changed to air, the absolute performances of the different MEAs decrease approximately 6% overall (Fig. 3), while the order of MEA performance remains the same as with O_2. The small decrease in performance is surprising as it is expected to be 20–35% with a supported Pt catalyst [84–86]. The SEM images of catalyst layer show a very open structure, which can facilitate the mass transfer and suppress the effect of decreased O_2 concentration (see Section 3.4). It could also be that the relatively large area of the N-FWCNTs compared to the scattered Pt-nanoparticles on an inactive carbon support allows for better access of O_2 to the active sites and thus the decrease in the O_2 concentration does not affect the N-FWCNT system as significantly. Finally, the sensitivity of Pt toward methanol crossover may be enhanced when the O_2 concentration is reduced and so the methanol tolerant N-FWCNTs [77] do not show such a large decrease in performance.

For easier comparison, the polarization curves of the optimum MEA40 with oxygen and air are shown in the same plot in Fig. 4. It can be seen that the performance of the air-DMFC decreases little more than that of O_2-DMFC at the high current density region, where mass transport losses are in a more significant role. The same can be seen with all the MEAs (not shown) indicating that the mass transfer limitations are due to the reduced oxygen content of the

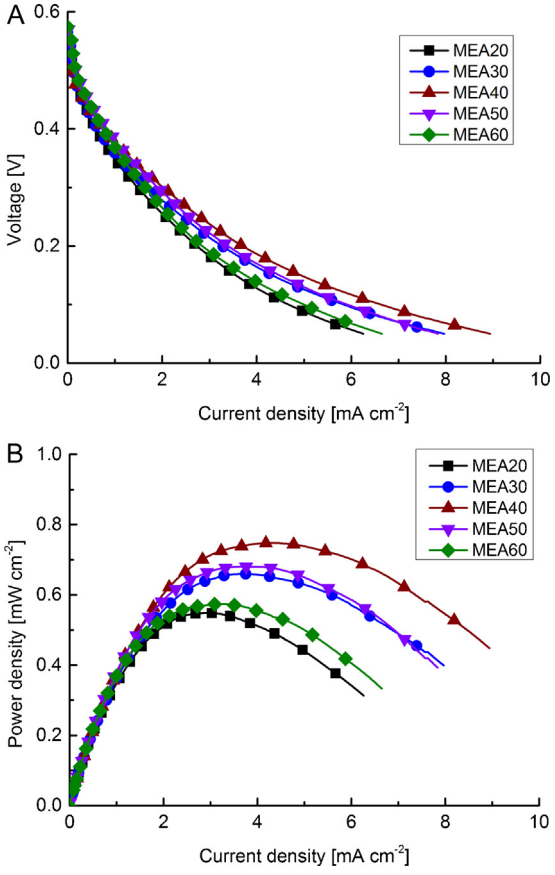

Fig. 2. The DMFC performance with the different FAA3 ionomer contents in the N-FWCNT cathode catalyst layer. The oxidant is O_2. (A) Voltage and (B) power density curves.

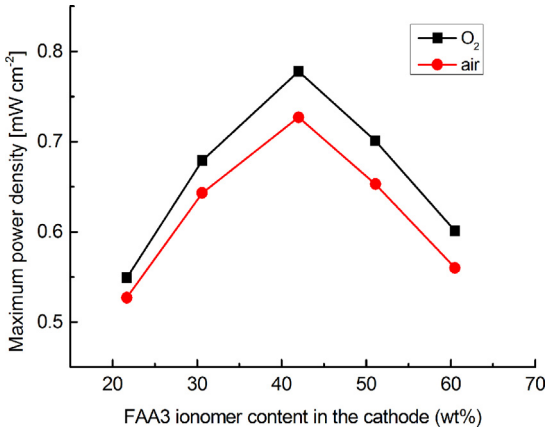

Fig. 3. DMFC maximum power density of the MEAs plotted against the FAA3 ionomer content in the cathode. The lines are for visual aid.

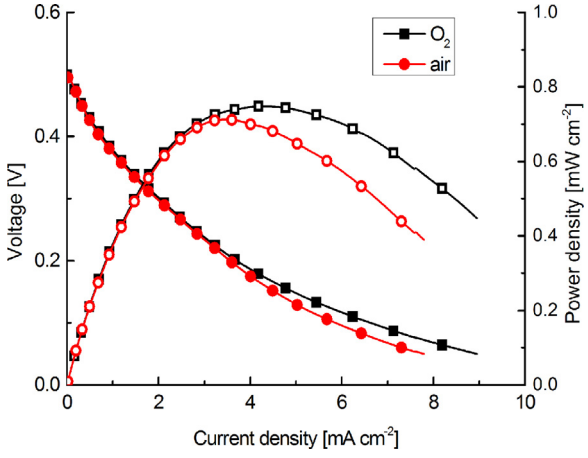

Fig. 4. Comparison between the DMFC polarization curves of MEA40 with O_2 and air as oxidants. The full symbols refer to voltage curves and open symbols to power curves.

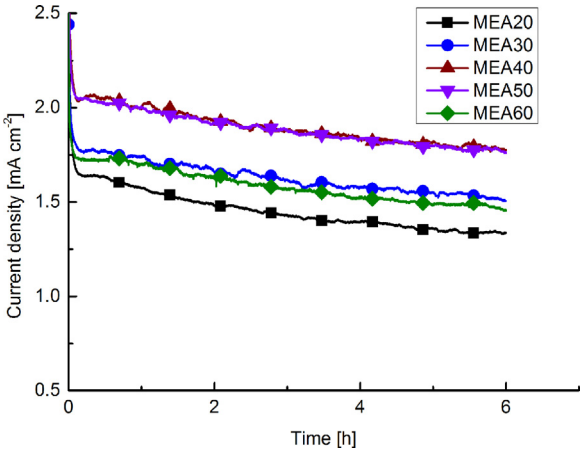

Fig. 5. 6-h constant voltage measurements at 0.2 V in DMFC.

oxidant and cannot be improved by changing the FAA3 content in the cathode.

The total ohmic resistance of the fuel cell was determined from the high frequency end of the impedance spectrum of each MEA (Table 1). Clearly, the resistance increased linearly from MEA30 to MEA60, while MEA20 showed the highest resistance. Since the thickness (Table 1) and therefore the resistance of the cathode should increase with the ionomer content, this indicates that the amount of FAA3 in MEA20 is not enough to make a good contact between the catalyst layer and the membrane, thus increasing the ionic contact resistance between them. This is especially important in this case as heat-pressing could not be used to improve the contact between the components due to the sensitivity of FAA3. Similar effect has been observed for Nafion-based DMFC anodes and cathodes with commercial unsupported [87] or carbon supported [88,89] PtRu catalysts. When the fuel cells were dismantled, it was noticed that the GDLs in MEA40, MEA50 and MEA60 were attached to the membrane during testing due to the compression from the end plates, while GDLs in MEA20 and MEA30 were still loose further demonstrating the requirement of a higher amount of FAA3 for a proper contact between the components.

Long term stability of the catalyst was studied by a 6-h chronoamperometric measurement at 0.2 V with oxygen as the oxidant (Fig. 5 and Table 1). It is evident that the FAA3 content has little effect on the stability of the fuel cell even though the absolute current values vary between the catalysts. This is unlike what was seen with Nafion and carbon nanofiber supported PtRu as DMFC anode, where the stability of the fuel cell increased until 70 wt% ionomer content [83]. The current decrease is slightly larger for MEA20 ($49\,\mu A\,cm^{-2}\,h^{-1}$) than for the other MEAs ($43 \pm 2\,\mu A\,cm^{-2}\,h^{-1}$), which could indicate that 20 wt% of FAA3 is not enough to bind the catalyst layer properly together resulting in quicker erosion and delamination during fuel cell use. The current decreases were calculated between the current at 0.5 h and at 6 h to eliminate the large and reversible drop at the start of the measurement [90].

3.3. Comparison between N-FWCNT and Pt cathode

After the optimization of N-FWCNT cathode catalyst layer, the performance of the best performing MEA40 was compared to a commercial carbon supported platinum (60 wt% Pt) catalyst (MEA-Pt). For the commercial cathode, 30 wt% of FAA3 was used according to the results of Carmo et al. [80] The polarization and power density curves of MEA40 and MEA-Pt are presented in Fig. 6. When O_2 is the oxidant, the performance of the catalysts are quite similar in the high current density region. However, at low current density MEA40 shows superior performance due to its considerably higher

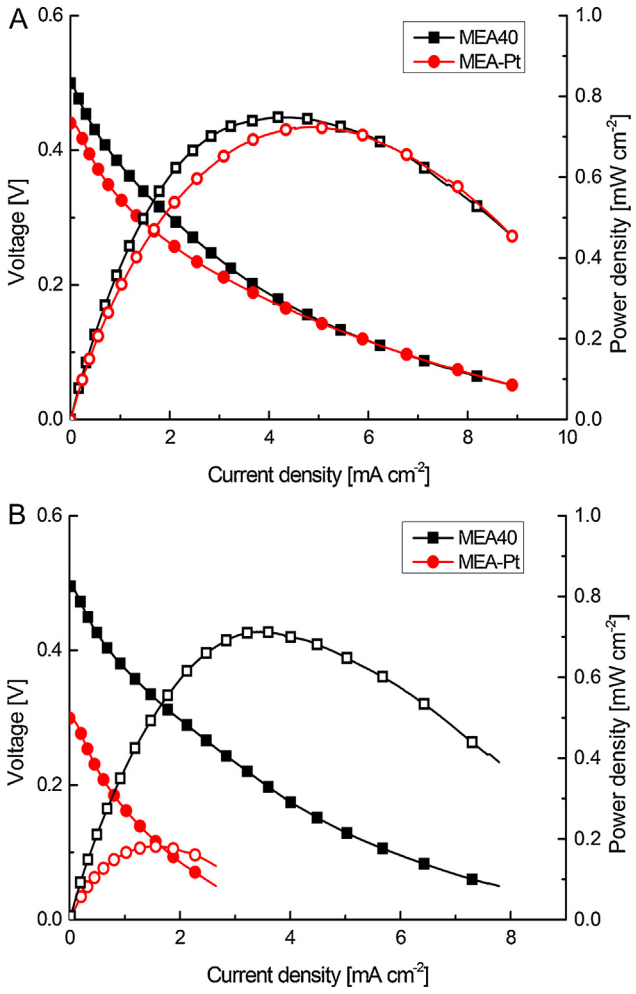

Fig. 6. The DMFC performance of the N-FWCNT cathode (MEA40, $2.3\,mg_{(N\text{-}FWCNT)}\,cm^{-2}$) and Pt/C cathode (MEA-Pt, $0.5\,mg_{(Pt)}\,cm^{-2}$). (A) O_2, (B) air as oxidant. The full symbols refer to voltage curves and open symbols to power curves.

open circuit voltage (OCV): 0.50 V and 0.44 V for MEA40 and MEA-Pt, respectively. This indicates that the N-FWCNTs are more tolerant to methanol [77] than the Pt-based catalyst, since the methanol crossing over the membrane from the anode causes a mixed potential at DMFC cathodes based on Pt and lowers the OCV strongly [5]. The maximum power density of MEA-Pt is $0.72\,mW\,cm^{-2}$, which is 92% that of MEA40 ($0.78\,mW\,cm^{-2}$). The power and current densities are relatively low compared to the results of Sun et al. [69] but this is due to the higher fuel cell temperature (60 °C) and the addition of KOH into their methanol fuel solution that radically improves the performance of an AAMFC [91]. We purposefully avoided using KOH solution as it negates the advantage of a solid electrolyte by introducing free cations into the system that can precipitate with carbonate ions produced from the anode reaction. They also used self-synthesized membrane from poly(arylene ether ketone) containing pendant quaternary ammonium groups and acidic Nafion as the ionomer in the catalyst layer, both of which will affect the performance. However, the DMFC power densities obtained here are 2.5 times higher compared to previous measurements with Fumatech FAA2 membrane at 30 °C with commercial carbon supported Pt-catalyst and PtRu-catalyst on the cathode and anode, respectively [92].

When the oxidant is changed to air, MEA40 performs remarkably better than MEA-Pt. The maximum power density of MEA-Pt is now $0.18\,mW\,cm^{-2}$, which is only 25% that of MEA40

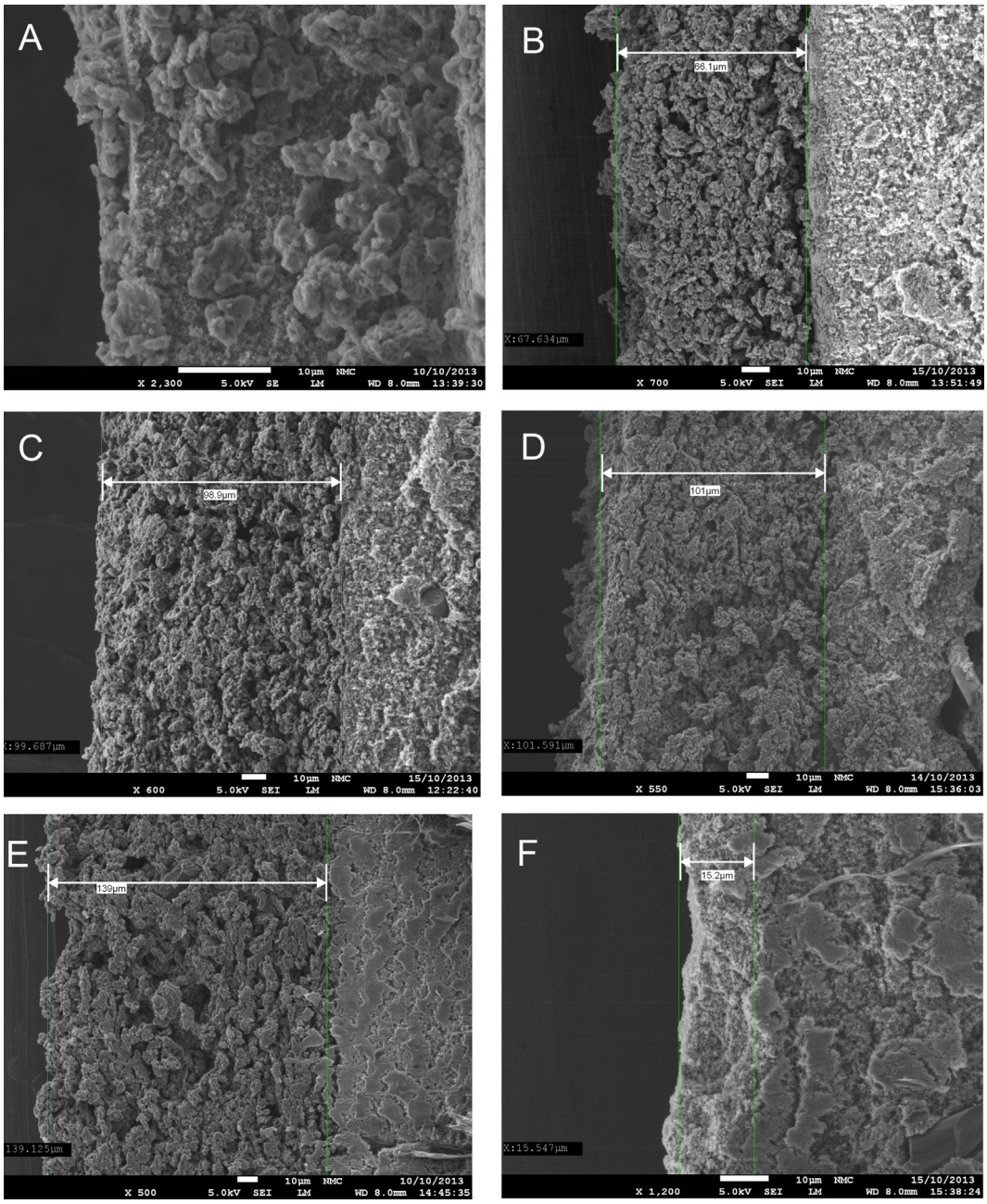

Fig. 7. SEM images of the cross-sections of the cathode catalyst layers. (A) MEA20, (B) MEA30, (C) MEA40, (D) MEA50, (E) MEA60 and (F) MEA-Pt.

(0.73 mW cm^{-2}). Taking into account the fact that there is more catalyst in MEA40, the mass specific power densities are 360 mW g(Pt)$^{-1}$ and 330 mW g(N-FWCNT)$^{-1}$ indicating N-FWCNTs are an excellent candidate to replace Pt as they only contain cheap and abundant elements (C and N). The relative power density decrease from O_2 is 75% for MEA-Pt, while it is only 6% for MEA40, which could be due to the catalyst layer structure and mass transfer differences between the MEAs (Section 3.4). In addition, the OCV drops radically for MEA-Pt from 0.44 to 0.30 V compared to O_2 measurement, while the OCV of MEA40 remains at 0.50 V. The large decreases both in OCV and power density for MEA-Pt imply that the lower O_2 concentration at the cathode allows the methanol crossover to disrupt the functioning of Pt-catalyst more significantly than when pure oxygen is used. In addition to the mixed potential and CO poisoning affecting the DMFC performance also with pure O_2, the extent of the decrease in performance is likely due to the fact that the methanol oxidation at the cathode consumes O_2, so the low 20% O_2 concentration in air is further reduced leaving an O_2 depleted and N_2 enriched area around the Pt catalyst particles. When pure O_2 is used, the relative drop in its concentration is not as large. On the other hand, when methanol tolerant N-FWCNTs [77] are used methanol simply diffuses out of the catalyst layer without reacting. Also, the open structure of MEA40 can help O_2 reach the active sites more easily, thus mitigating the effect of O_2 concentration reduction (Section 3.4).

The effect of methanol to the fuel cell performance was further examined by replacing the methanol solution with H_2 as the fuel. In this case, when O_2 was changed to air, the performance loss was 6% for MEA40 and 21% for MEA-Pt (measured at 0.3 V due to Ru oxidation at the anode coinciding with the maximum power density). For MEA40, this decrease is the same as with methanol but for MEA-Pt it is only less than a third indicating that methanol

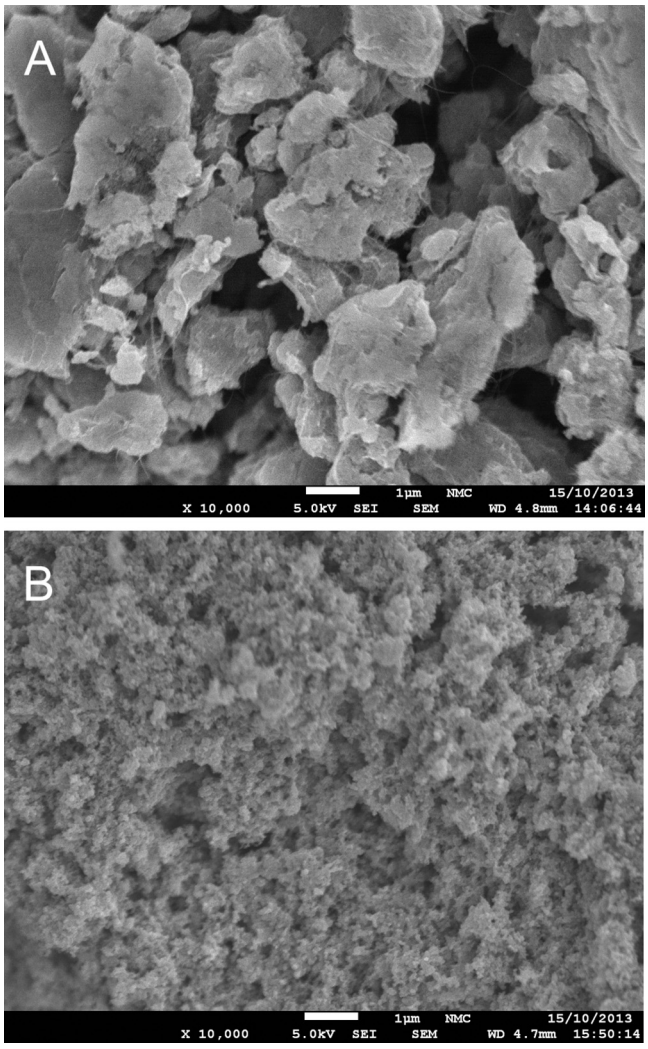

Fig. 8. Higher magnification (10,000×) of the cathode catalyst layers of (A) MEA30 (31 wt% FAA3) and (B) MEA-Pt (29 wt% FAA3).

is an important factor in the surprisingly low performance of the MEA-Pt with methanol and air. Also, the OCV of MEA-Pt was higher than MEA40 with the H_2 fuel and both OCVs decreased about 30 mV when O_2 was switched to air. However, MEA40 still shows better performance with O_2 and clearly superior performance with air: the current for MEA-Pt at 0.3 V is 98% of MEA40 with O_2 and 83% with air. The H_2 fuel cell was not further studied due to the PtRu catalyst on the anode, which is not optimal for the H_2 fuel.

3.4. Cathode catalyst structure

In order to further investigate the effect of FAA3 on the catalyst layer structure with N-FWCNTs and the Pt-catalyst, SEM images of the MEA cathodes were taken (Figs. 7a–f and 8a–b). In the case of MEA20, the whole catalyst layer peeled off in small pieces as it was removed from the fuel cell and cut for SEM imaging. Only small flakes of the catalyst can be seen on the microporous carbon layer of the GDL in the SEM image (Fig. 7a). Therefore, there is no structure or thickness data for MEA20.

Generally, the N-FWCNT based catalyst layers show large voids in their structure compared to the commercial catalyst with a Vulcan-like carbon support (Fig. 8), which also makes the catalyst layer relatively thick compared to MEA-Pt: the average cathode thickness of MEA-Pt is 19 μm, while it is 80 μm thick in MEA30 with about the same FAA3 content. Mass-transfer should be facilitated in thinner catalyst layers as the traversed lengths are smaller but when MEA40 and MEA-Pt are compared, the 6 times thicker catalyst layer in MEA40 results in better performance. Therefore it can be concluded that the thickness of the catalyst layer is not limiting factor with N-FWCNTs most likely due to the open structure.

It appears that due to the surface charge caused by nitrogen incorporation into the FWCNT structure [11], the charged ionomer is attracted around the N-FWCNT bundles and forms aggregates. The large voids are beneficial for facilitated mass transfer through the layer, not only for O_2 to get to the active sites but also for water management of the cathode. Water produced at the cathode of acidic DMFCs and permeating from the anode is a significant factor causing flooding of the catalyst layer and blocking of the catalyst sites. Although there is no water produced at the cathode in the alkaline DMFC, the water permeating from cathode can block catalyst sites of the cathode [93]. The large voids enhance the water removal as there is more space for the water to flow out and it also remains as vapor more easily in larger pores [94]. The voids appear to be slightly more blocked at the high FAA3 contents and the aggregates are bigger, which can contribute to the lower performance due to the decreased mass transfer for MEA50 and MEA60. However, it is clear that FAA3 does not fill the voids evenly but attaches to the already present aggregates. Therefore, the structure of the catalyst layer remains remarkably open, which is an interesting feature enabling the use of high amounts of ionomer in the catalyst layer without hindering mass transfer completely. This effect should also be studied further with other membrane and ionomer materials; however, this is out of the scope of this investigation. Finally, as more FAA3 gathers around the N-FWCNT bundles, they may become more blocked from O_2 so that they become inactive for ORR reducing the efficiency of the fuel cell, as seen with MEA50 and MEA60. Similar aggregates can also be observed with undoped FWCNT-PtRu and Nafion ionomer [95], but the voids are smaller and more blocked even with low Nafion concentration (30 wt%) and especially so after DMFC testing.

As the total resistance of the fuel cell with MEA-Pt is higher than with MEA30 to MEA60 despite the greatly reduced thickness (Table 1), it can be concluded that N-FWCNTs decrease the contact and/or catalyst layer resistances in the MEAs.

The absolute determination of the catalyst layer thicknesses of each MEA is difficult, because part of the catalyst layer had attached to the membrane during the testing. This is reflected in the large error margins of the results (Table 1). However, the general trend shows increasing thickness with increasing FAA3 content: from MEA30 to MEA40 the thickness increases significantly, then a slight decrease was observed with MEA50 and finally the thickest catalyst layer was found in MEA60. Surprisingly, this suggests that even though the mass of the ionomer increases exponentially with its weight percentage in the electrode layer, the thickness of the catalyst layer does not. Apparently, FAA3 partly fills the voids found in the catalyst layer as its amount is increased beyond 40 wt%.

4. Conclusions

In this work, alkaline anion-exchange membrane DMFC performance was investigated with a commercially available Fumatech FAA3 membrane and ionomer with Pt-free nitrogen-doped few-walled carbon nanotubes as the cathode catalyst. The optimum ionomer content of the cathode catalyst layer was found to be 40 wt% in the range of 20–60 wt% in terms of power and current densities. The ionomer content did not have a significant effect on the DMFC stability for concentrations higher than 30 wt%.

The N-FWCNTs were compared to a commercial carbon supported Pt as the cathode catalyst and remarkably, they were found

to perform 4 times better than the commercial catalyst while air was used as the oxidant. The performance differences were attributed to the methanol tolerance of the N-FWCNTs and the more open electrode structure.

The examination of the catalyst layer structure with scanning electron microscopy revealed that the FAA3 ionomer formed aggregates around the N-FWCNTs leaving the catalyst layer full of voids, which should facilitate the availability of O_2 through the whole catalyst layer. In comparison, the Pt catalyst layer was dense with smaller voids, which are less likely to percolate through the whole layer.

This study shows that N-FWCNTs are an excellent and cheap oxygen reduction catalyst in alkaline fuel cell conditions and they can clearly outperform an expensive, commercial Pt catalyst in the presence of methanol with air as the oxidant. The results are also significant compared to common investigations on new fuel cell catalysts, which only focus on the catalytic activity, in that here we show that MEA fabrication and study of fuel cell catalyst layer structure from novel materials is important and can reveal additional advantageous features like the open layer structure formed with the N-FWCNTs.

Acknowledgements

The authors would like to thank the following instances for funding: Aalto University Starting Grant and MIDE (T.K.), Alfred Kordelin Foundation (P.K.), the Academy of Finland (M.B. and V.R.) and TEKES (E.P.). This work made use of the Aalto University Nanomicroscopy Center (Aalto-NMC) premises.

References

[1] X. Zhao, M. Yin, L. Ma, L. Liang, C. Liu, J. Liao, T. Lu, W. Xing, Energy Environ. Sci. 4 (2011) 2736–2753.
[2] F. Lufrano, V. Baglio, P. Staiti, V. Antonucci, A.S. Aricó, J. Power Sources 243 (2013) 519–534.
[3] I.E.L. Stephens, A.S. Bondarenko, U. Gronbjerg, J. Rossmeisl, I. Chorkendorff, Energy Environ. Sci. 5 (2012) 6744–6762.
[4] Y. Shao, G. Yin, Y. Gao, J. Power Sources 171 (2007) 558–566.
[5] M. Ahmed, I. Dincer, Int. J. Energy Res. 35 (2011) 1213–1228.
[6] Z. Yang, H. Nie, X. Chen, X. Chen, S. Huang, J. Power Sources 236 (2013) 238–249.
[7] M. Watanabe, D.A. Tryk, M. Wakisaka, H. Yano, H. Uchida, Electrochim. Acta 84 (2012) 187–201.
[8] F. Jaouen, E. Proietti, M. Lefevre, R. Chenitz, J. Dodelet, G. Wu, H.T. Chung, C.M. Johnston, P. Zelenay, Energy Environ. Sci. 4 (2011) 114–130.
[9] N. Cheng, C. Kemna, S. Goubert-Renaudin, A. Wieckowski, Electrocatalysis 3 (2012) 238–251.
[10] L. Qu, Y. Liu, J. Baek, L. Dai, ACS Nano 4 (2010) 1321–1326.
[11] K. Gong, F. Du, Z. Xia, M. Durstock, L. Dai, Science 323 (2009) 760–764.
[12] S. Maldonado, K.J. Stevenson, J. Phys. Chem. B 109 (2005) 4707–4716.
[13] J. Bai, Q. Zhu, Z. Lv, H. Dong, J. Yu, L. Dong, Int. J. Hydrogen Energy 38 (2013) 1413–1418.
[14] Z. Mo, S. Liao, Y. Zheng, Z. Fu, Carbon 50 (2012) 2620–2627.
[15] W. Yang, T. Fellinger, M. Antonietti, J. Am. Chem. Soc. 133 (2011) 206–209.
[16] M. Vikkisk, I. Kruusenberg, U. Joost, E. Shulga, K. Tammeveski, Electrochim. Acta 87 (2013) 709–716.
[17] X. Li, G. Liu, B.N. Popov, J. Power Sources 195 (2010) 6373–6378.
[18] T. Xing, J. Sunarso, W. Yang, Y. Yin, A.M. Glushenkov, L.H. Li, P.C. Howlett, Y. Chen, Nanoscale 5 (2013) 7970–7976.
[19] X. Zhou, Z. Yang, H. Nie, Z. Yao, L. Zhang, S. Huang, J. Power Sources 196 (2011) 9970–9974.
[20] Z. Wang, R. Jia, J. Zheng, J. Zhao, L. Li, J. Song, Z. Zhu, ACS Nano 5 (2011) 1677–1684.
[21] D. Yu, Q. Zhang, L. Dai, J. Am. Chem. Soc. 132 (2010) 15127–15129.
[22] R. Liu, D. Wu, X. Feng, K. Muellen, Angew. Chem. Int. Ed. 49 (2010) 2565–2569, S2565/1–S2565/6.
[23] D. Yu, L. Wei, W. Jiang, H. Wang, B. Sun, Q. Zhang, K. Goh, R. Si, Y. Chen, Nanoscale 5 (2013) 3457–3464.
[24] Z. Lu, S. Bao, Y. Gou, C. Cai, C. Ji, M. Xu, J. Song, R. Wang, RSC Adv. 3 (2013) 3990–3995.
[25] B. Zheng, J. Wang, F. Wang, X. Xia, Electrochem. Commun. 28 (2013) 24–26.
[26] J. Wu, D. Zhang, Y. Wang, B. Hou, J. Power Sources 227 (2013) 185–190.
[27] S.M. Unni, S. Devulapally, N. Karjule, S. Kurungot, J. Mater. Chem. 22 (2012) 23506–23513.
[28] Z. Lin, G. Waller, Y. Liu, M. Liu, C. Wong, Adv. Energy Mater. 2 (2012) 884–888.
[29] L. Lai, J.R. Potts, D. Zhan, L. Wang, C.K. Poh, C. Tang, H. Gong, Z. Shen, J. Lin, R.S. Ruoff, Energy Environ. Sci. 5 (2012) 7936–7942.
[30] Y. Sun, C. Li, G. Shi, J. Mater. Chem. 22 (2012) 12810–12816.
[31] Z. Lin, M. Song, Y. Ding, Y. Liu, M. Liu, C. Wong, Phys. Chem. Chem. Phys. 14 (2012) 3381–3387.
[32] Z. Sheng, L. Shao, J. Chen, W. Bao, F. Wang, X. Xia, ACS Nano 5 (2011) 4350–4358.
[33] D. Geng, Y. Chen, Y. Chen, Y. Li, R. Li, X. Sun, S. Ye, S. Knights, Energy Environ. Sci. 4 (2011) 760–764.
[34] Y. Qiu, J. Yin, H. Hou, J. Yu, X. Zuo, Electrochim. Acta 96 (2013) 225–229.
[35] T. Sharifi, G. Hu, X. Jia, T. Waagberg, ACS Nano 6 (2012) 8904–8912.
[36] H. Li, H. Liu, Z. Jong, W. Qu, D. Geng, X. Sun, H. Wang, Int. J. Hydrogen Energy 36 (2011) 2258–2265.
[37] D. Higgins, Z. Chen, Z. Chen, Electrochim. Acta 56 (2010) 1570–1575.
[38] D. Geng, H. Liu, Y. Chen, R. Li, X. Sun, S. Ye, S. Knights, J. Power Sources 196 (2011) 1795–1801.
[39] C.V. Rao, C.R. Cabrera, Y. Ishikawa, J. Phys. Chem. Lett. 1 (2010) 2622–2627.
[40] Z. Chen, D. Higgins, Z. Chen, Carbon 48 (2010) 3057–3065.
[41] T.C. Nagaiah, S. Kundu, M. Bron, M. Muhler, W. Schuhmann, Electrochem. Commun. 12 (2010) 338–341.
[42] Z. Chen, D. Higgins, H. Tao, R.S. Hsu, Z. Chen, J. Phys. Chem. C 113 (2009) 21008–21013.
[43] S. Kundu, T.C. Nagaiah, W. Xia, Y. Wang, D. Van Stefan, J.H. Bitter, M. Santa, G. Grundmeier, M. Bron, W. Schuhmann, M. Muhler, J. Phys. Chem. C 113 (2009) 14302–14310.
[44] J. Yin, Y. Qiu, J. Yu, J. Electroanal. Chem. 702 (2013) 56–59.
[45] J. Yin, Y. Qiu, J. Yu, Chem. Lett. 42 (2013) 413–415.
[46] Y. Qiu, J. Yu, T. Shi, X. Zhou, X. Bai, J.Y. Huang, J. Power Sources 196 (2011) 9862–9867.
[47] E.J. Biddinger, D. Deak, U.S. Ozkan, Top. Catal. 52 (2009) 1566–1574.
[48] N. Gavrilov, I.A. Pasti, M. Mitric, J. Travas-Sejdic, G. Ciric-Marjanovic, S.V. Mentus, J. Power Sources 220 (2012) 306–316.
[49] H. Zhong, H. Zhang, Z. Xu, Y. Tang, J. Mao, ChemSusChem 5 (2012) 1698–1702, S1698/1–S1698/2.
[50] Y.M. Yu, J.H. Zhang, C.H. Xiao, J.D. Zhong, X.H. Zhang, J.H. Chen, Fuel Cells (Weinheim, Ger.) 12 (2012) 506–510.
[51] Y. Li, T. Li, M. Yao, S. Liu, J. Mater. Chem. 22 (2012) 10911–10917.
[52] F. Zheng, G. Mu, Z. Zhang, Y. Shen, M. Zhao, G. Pang, Mater. Lett. 68 (2012) 453–456.
[53] G. Ma, R. Jia, J. Zhao, Z. Wang, C. Song, S. Jia, Z. Zhu, J. Phys. Chem. C 115 (2011) 25148–25154.
[54] S. Chen, J. Bi, Y. Zhao, L. Yang, C. Zhang, Y. Ma, Q. Wu, X. Wang, Z. Hu, Adv. Mater. (Weinheim Ger.) 24 (2012) 5593–5597.
[55] H. Li, W. Kang, L. Wang, Q. Yue, S. Xu, H. Wang, J. Liu, Carbon 54 (2013) 249–257.
[56] N. Brun, S.A. Wohlgemuth, P. Osiceanu, M.M. Titirici, Green Chem. 15 (2013) 2514–2524.
[57] S. Wohlgemuth, T. Fellinger, P. Jaeker, M. Antonietti, J. Mater. Chem. A 1 (2013) 4002–4009.
[58] Z. Mo, H. Peng, H. Liang, S. Liao, Electrochim. Acta 99 (2013) 30–37.
[59] Y. Liu, S. Chen, X. Quan, H. Yu, H. Zhao, Y. Zhang, G. Chen, J. Phys. Chem. C 117 (2013) 14992–14998.
[60] V. Nallathambi, J. Lee, S.P. Kumaraguru, G. Wu, B.N. Popov, J. Power Sources 183 (2008) 34–42.
[61] G. Wu, M. Nelson, S. Ma, H. Meng, G. Cui, P.K. Shen, Carbon 49 (2011) 3972–3982.
[62] T. Onodera, S. Suzuki, T. Mizukami, H. Kanzaki, J. Power Sources 196 (2011) 7994–7999.
[63] H. Oh, J. Oh, W.H. Lee, H. Kim, H. Kim, Int. J. Hydrogen Energy 36 (2011) 8181–8186.
[64] G. Liu, X. Li, P. Ganesan, B.N. Popov, Electrochim. Acta 55 (2010) 2853–2858.
[65] A. Dorjgotov, J. Ok, Y. Jeon, S. Yoon, Y. Shul, J. Solid State Electrochem. 17 (2013) 2567–2577.
[66] R. Venkateswara Chitturi, Y. Ishikawa, J. Phys. Chem. C 116 (2012) 4340–4346.
[67] D.C. Higgins, Z. Chen, ECS Trans. 28 (2010) 63–68.
[68] J. Kim, S. Lim, S. Kim, D. Peck, B. Lee, S. Yoon, D. Jung, J. Nanosci. Nanotechnol. 11 (2011) 6350–6358.
[69] X. Sun, P. Song, Y. Zhang, C. Liu, W. Xu, W. Xing, Sci. Rep. 3 (2013).
[70] E.H. Yu, U. Krewer, K. Scott, Energies (Basel Switz.) 3 (2010) 1499–1528.
[71] E.H. Yu, X. Wang, U. Krewer, L. Li, K. Scott, Energy Environ. Sci. 5 (2012) 5668–5680.
[72] D. von Dieter, D. Singh, J.C. King, U.S. Ozkan, Appl. Catal. B 113–114 (2012) 126–133.
[73] P.V. Mazin, N.A. Kapustina, M.R. Tarasevich, Russ. J. Electrochem. 47 (2011) 275–281.
[74] S.Q. Ci, Y.M. Wu, J.P. Zou, L.H. Tang, S.L. Luo, J.H. Li, Z.H. Wen, Chin. Sci. Bull. 57 (2012) 3065–3070.
[75] L. Feng, Y. Yan, Y. Chen, L. Wang, Energy Environ. Sci. 4 (2011) 1892–1899.
[76] T. Hibino, K. Kobayashi, P. Heo, Electrochim. Acta 112 (2013) 82–89.
[77] M. Borghei, P. Kanninen, M. Lundahl, I. Anoshkin, T. Susi, J. Sainio, A. Nasibulin, T. Kallio, K. Tammeveski, E. Kauppinen, V. Ruiz, Appl. Catal. B (2014) (submitted for publication).
[78] E.G. Rakov, D.A. Grishin, Y.V. Gavrilov, E.V. Rakova, A.G. Nasibulin, H. Jiang, E.I. Kauppinen, Russ. J. Electrochem. 78 (2004) 1966–1971.
[79] G. Wu, D. Li, C. Dai, D. Wang, N. Li, Langmuir 24 (2008) 3566–3575.
[80] M. Carmo, G. Doubek, R.C. Sekol, M. Linardi, A.D. Taylor, J. Power Sources 230 (2013) 169–175.
[81] W. Li, M. Waje, Z. Chen, P. Larsen, Y. Yan, Carbon 48 (2010) 995–1003.

[82] K. Jeng, C. Chien, N. Hsu, W. Huang, S. Chiou, S. Lin, J. Power Sources 164 (2007) 33–41.
[83] P. Kanninen, M. Borghei, V. Ruiz, E.I. Kauppinen, T. Kallio, Int. J. Hydrogen Energy 37 (2012) 19082–19091.
[84] A.K. Shukla, C.L. Jackson, K. Scott, R.K. Raman, Electrochim. Acta 47 (2002) 3401–3407.
[85] K. Scott, E. Yu, G. Vlachogiannopoulos, M. Shivare, N. Duteanu, J. Power Sources 175 (2008) 452–457.
[86] S.H. Seo, C.S. Lee, Energy Fuels 22 (2008) 1212–1219.
[87] X. Zhao, X. Fan, S. Wang, S. Yang, B. Yi, Q. Xin, G. Sun, Int. J. Hydrogen Energy 30 (2005) 1003–1010.
[88] X. Xue, C. Bock, L. Birry, B.R. MacDougall, Fuel Cells (Weinheim, Ger.) 11 (2011) 286–300.
[89] B. Krishnamurthy, S. Deepalochani, K.S. Dhathathreyan, Fuel Cells (Weinheim, Ger.) 8 (2008) 404–409.
[90] H. Cha, C. Chen, J. Shiu, J. Power Sources 192 (2009) 451–456.
[91] C. Coutanceau, L. Demarconnay, C. Lamy, J.-M. Léger, J. Power Sources 156 (2006) 14–19.
[92] A. Santasalo-Aarnio, S. Hietala, T. Rauhala, T. Kallio, J. Power Sources 196 (2011) 6153–6159.
[93] A. Brouzgou, A. Podias, P. Tsiakaras, J. Appl. Electrochem. 43 (2013) 119–136.
[94] C.S. Kong, D. Kim, H. Lee, Y. Shul, T. Lee, J. Power Sources 108 (2002) 185–191.
[95] A. Santasalo-Aarnio, M. Borghei, I.V. Anoshkin, A.G. Nasibulin, E.I. Kauppinen, V. Ruiz, T. Kallio, Int. J. Hydrogen Energy 37 (2012) 3415–3424.